Journal of The Electrochemical Society, **166** (10) A2013-A2020 (2019)
0013-4651/2019/166(10)/A2013/8/$38.00 © The Electrochemical Society

Silicon Nanoparticles Confined in Thin Carbon Network: The Free-Standing Anode of Lithium Ion Batteries with High Performance and Easy Recyclability

Junhua Kong [1,z] **and Yuefan Wei** [2]

[1] *Institute of Materials Research and Engineering, a-star, Singapore 138634*
[2] *School of Mechanical and Aerospace Engineering, Nanyang Technological University, Singapore 639798*

Si is a promising anode candidate of lithium ion batteries with exceptionally high theoretical capacity, however, has fatal issues including large volume expansion-induced instability and poor electrical conduction during the charging/discharging process. The stabilization of the Si anode through buffering its volume expansion meanwhile maintaining its structure/morphology integrity is currently the major strategy to overcome the issues. In this work, commercially available Si nanoparticles were confined within the network of thin graphitized carbon layer (from carbonized polydopamine, named as C-PDA) through a straightforward route, forming freestanding flexible and robust mat that can be used as anode directly. Excellent electrochemical performance, i.e., high cycled capacity (about 1750 mAh g^{-1} after 100 cycles at 100 mA g^{-1}) and rate capacity (around 1600 ∼ 1700, 1200 ∼ 1300, 800 ∼ 900 and 600 ∼ 700 mAh g^{-1} at 200, 500, 1000 and 2000 mA g^{-1}, respectively), was achieved after optimization due to the C-PDA thin layer that creates electron conduction pathway and the interconnected channels within the C-PDA network that offers free diffusion of electrolyte solution thus smooth transportation of Li ions. Unlike the common sense of accommodating/buffering the volume expansion of Si by carbon phase, the Si NPs collapse into smaller ones upon lithiation at the initial stage and are still trapped within the respective C-PDA frames. The C-PDA network acts as interlock to stabilize the collapsed Si, leading to good electrochemical properties. Recyclability of the used anode was also investigated in this work, implying that taking the advantage of its freestanding nature with no binder and conductive agent used, the used Si NPs with smaller size and maintained crystallinity can be easily recycled through simple solvent soaking after discharge/charge cycling. This work offers a unique and useful strategy of utilizing Si materials in an environment friendly and cost-effective way for energy storage application.
 [DOI: 10.1149/2.1021910jes]

Manuscript submitted April 15, 2019; revised manuscript received May 17, 2019. Published June 13, 2019.

As the one with exceptionally high gravimetric and volumetric capacity, low discharge voltage as well as abundant resource, silicon (Si) is a promising anode candidate as potential alternative to current commercial graphite in lithium ion batteries (LIBs). The exploration of Si-based anodes has been extensively carried out, as evidenced by hundreds of scientific papers published in the last 15 years and having been reviewed from varied perspectives.[1–7] Despite the great potential, several issues of Si as anode severely hinder its practical use, including large volume expansion (more than 300% upon full lithiation) that irreversibly breaks the structural integrity, poor intrinsic electrical conductivity that causes sluggish electrochemical kinetics, as well as gradual pulverization of the anode along with lithiation/de-lithiation cycles.

Typical strategies to tackle the above issues mainly rely on stabilizing the Si nanostructure while maintaining its morphology/structure integrity during lithiation/de-lithiation. Firstly, introducing "nano-effect" by reducing at least one dimension of Si to normally less than 100 nm, such as Si nanoparticles/nanospheres/nanoflowers,[8–10] nanocubes,[11] mesoporous Si,[12–14] Si nanowires,.[15–18] The nanoscale dimension of the Si realizes faster and more complete alloying and de-alloying with lithium ions, and meanwhile suppresses the volume expansion during the process. Secondly, combining with structurally stable and electrically conductive components to produce Si-based composites. Among all the candidates (metals, polymers, etc.),[19–22] carbon is the most promising one, acting as host/support of Si, that is capable of buffering/accommodating the volume change of Si during charging/discharging, as well as providing good electrical conduction to the composites. In addition, the carbon phase is also electrochemically active and contributes to the overall battery performance. So far, carbon nanofibers/carbon nanotubes,[23–25] graphene/graphite,[26–31] amorphous/doped carbon[32–36] have been synergistically introduced into Si nanostructures. The ratio of Si/carbon in the composites and the effectiveness of the interaction between Si and carbon are the critical factors that determine the properties. Last but not the least, improving the fabrication/assembling process through, for instance, optimizing the binders,[37–39] inkjet-printing of the anode,[40] etc. Overall, the design/development of proper Si nanocomposites that could efficiently utilize the electrochemical activity of Si is still highly desired.

[z]E-mail: kongjh@imre.a-star.edu.sg

Nowadays, the recyclability of the used materials has been becoming a more and more important consideration in industry that favors the utilization efficiency of the materials and the environment protection. Yet this has rarely been investigated in the area of batteries, which the authors think it is worthwhile to unveil to add additional value to the good energy storage performance. In this work, we proposed a straightforward strategy to utilize Si via binding commercially available Si nanoparticles (NPs) within fibrous thin carbon network, achieving freestanding anode without the usage of any binder and carbon black. Interestingly, the Si NPs collapse into smaller ones instead of expanding in volume upon lithiation, leading to excellent electrochemical properties. Moreover, the used collapsed Si NPs can be easily recycled from the anode after battery test, offering opportunity for the further reuse of the Si material.

Experimental

Materials.—Si nanoparticles (Si NPs, APS ≤ 100 nm) were obtained from Alfa Aesar (USA). Dimethylformamide (DMF), polystyrene (PS, M_w = 350 000), dopamine hydrochloride (DOPA) and tris(hydroxymethyl)aminomethane (Tris) were purchased from Sigma-Aldrich (USA). The electrolyte solution, 1 M lithium hexafluorophosphate ($LiPF_6$) in a mixture of ethylene carbonate (EC) and dimethyl carbonate (DMC) with volume ratio of 1:1, and the lithium foil were purchased from Charslton Technologies, Pte., Ltd. (Singapore). All chemicals were used without further purification.

Preparation of porous PS/Si fibers.—Si NPs were homogeneously dispersed in DMF (10 wt%) through vigorous probe ultrasonication. PS was then dissolved in above Si/DMF suspension with concentration of 15 wt% through stirring at 60°C. The viscous PS/Si/DMF suspension was electrospun into PS/Si nanofibers, which were collected in ethanol to form a loose lump from 2 hrs electrospinning, under the applied voltage of 13 kV, feeding rate of 0.5 mL/hr and environmental humidity of around 60 H%. It is highlighted here that the ethanol acts as the collection medium for PS/Si fibers due to that PS is not soluble in ethanol yes has good compatibility and wettability in this solvent. The timely precipitation of the electrospun PS/Si fibers into ethanol forms loose lump of the fibers with large inter-fiber spaces.[41]

Preparation of Si encapsulated in thin carbon.—The electrospun PS/Si nanofibers that suspended in ethanol were washed with DI H_2O several times to fully replace ethanol, and then transferred into 300 mL DOPA aqueous solution with concentration of 0.5 mg/mL. 0.363 g Tris powder was then added and dissolved in above solution under shaking to initiate the in-situ polymerization of DOPA on the surface of the nanofibers for polydopamine (PDA) coating. The polymerization was running for 2 hrs before the coated nanofibers were washed by DI H_2O. Multiple in-situ polymerization using the fresh DOPA/Tris solution was conducted following the above procedure. After coating and drying under vacuum at 60°C, the samples were thermally treated in Ar atmosphere under the following condition: heating to 700°C at a heating rate of 3°C/min, and keeping at 700°C for 3 hrs. Corresponding to the coating times of 2, 4 and 6, the thermally treated samples are denoted as C-PDA/Si-2t, C-PDA/Si-4t and C-PDA/Si-6t, respectively.

Structural, morphological and electrochemical characterization.—A field-emission scanning electron microscope (FESEM, JEOL-7600F) and a high-resolution transmission electron microscope (HRTEM, JEOL-2100F) was used to study the morphologies and structures of the samples. Energy dispersive X-ray-scanning transmission electron microscope (EDX-STEM) elemental mapping was conducted to identify the element distribution. An X-ray diffractometer (XRD, Bruker D8 Discover GADDS), a thermogravimetric analyzer (TGA, Q500), an X-ray photoelectron spectroscopy (XPS, Theta-probe, Thermo Scientific) and a Fourier transform infrared spectroscope (FTIR, Shimadzu) was used to characterize the structures and composition. For the electrochemical properties evaluation, the thermally treated freestanding samples were cut into round shape with diameter of 10 mm and used as anodes of LIBs directly without using any binder and electrically conductive agent. To assemble the batteries, the anode, mesoporous monolayer membrane (Celgard 2500, USA, pre-wetting by soaking in electrolyte solution for a short term), the lithium foil and the electrolyte solution was put into CR2032 coin cell in an argon-filled glove box with moisture and oxygen level of less than 0.1 ppm. The assembled coin cell was connected to a battery test system (4200, MACCOR, for cycled and rate capacity measurement) or an electrochemical workstation (PGSTAT 302, Autolab, for cyclic voltammetric (CV) and electrochemical impedance spectroscopy (EIS) test) for electrochemical properties evaluation.

Results and Discussion

Morphologies and structures of Si NPs in C-PDA network.—Si in powder form is normally blended with carbon black to achieve electrical conduction, and bound by polymeric binder in order to paste the formed slurry onto the current collector. While from our strategy as shown schematically in Scheme 1, the commercially available Si NPs with average size of less than 100 nm are trapped within thin carbon network that is in freestanding form. Si NPs were firstly homogeneously dispersed in PS/DMF solution. After electrospinning, PS fibers with Si NPs embedded were produced. As shown in Figure 1a, bead-less fibers with diameter of 1∼3 μm were obtained. Under the high environmental humidity of above 50 H% during electrospinning, porous fibers were obtained as reported previously,[42] with large quantity of mesopores and some macropores located on the surface (Figure 1b). A SEM cross sectional view of a single PS/Si fiber, as shown in Figure 1c, confirms that within the fiber, interconnected nanochannels with size of tens of nanometers are created. The formed highly porous PS network in the fiber, confines the Si NPs through fully encapsulating them as typically indicated by the red arrows in Figure 1c. The inset TEM image of Figure 1c shows the edge area of a PS/Si fiber, further confirming that individual Si NPs are embedded within PS without aggregation.

PDA thin layer, acting as carbon source, was then deposited onto the surface of PS network. The open pores on the surface of fibers as well as the large interconnected nanochannels within the fibers allow facile diffusion of monomer aqueous solution thus even and complete PDA coating.[43,44] The thickness of the PDA thin layer varies and is

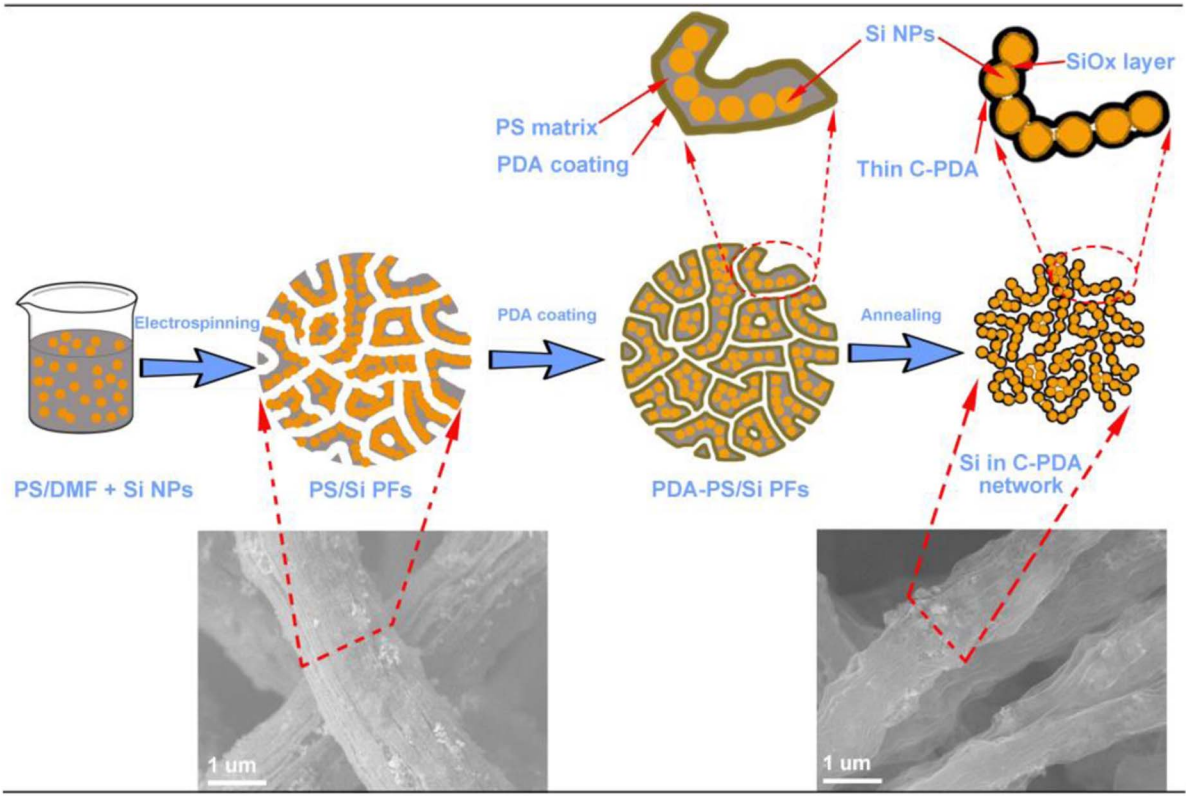

Scheme 1. The strategy to confine Si nanoparticles within thin carbon fibrous network (from SEM cross sectional view of the corresponding samples).

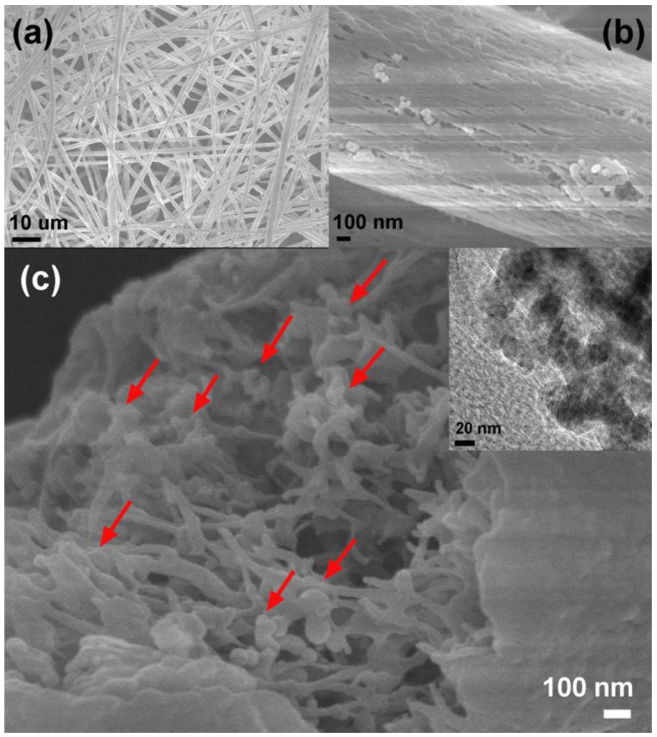

Figure 1. (a) and (b) SEM images of the PS/Si fibers, (c) SEM cross sectional view of a single fiber, showing the high porosity as well as the embedded Si NPs that pointed by red arrows. The inset of (c) shows the TEM image of the edge area of a single PS/Si fiber.

controlled by the coating times, which in turn brings different carbon contents for the final hybrids. After thermal treatment in argon, PDA was converted into graphitized carbon named as C-PDA,[45] while PS is totally removed via full degradation. Taking the one from 4 times PDA coating as an example (C-PDA/Si-4t), the fibrous morphology remains after thermal treatment (Figure 2a). The long fibers entangle with each other, forming non-woven mat which is flexible and strong enough to sustain battery assembling due to the robust thin C-PDA network (inset of Figure 2a). The diameter of the fibers is reduced to around 1 μm since the C-PDA thin layer shrinks upon the removal of PS matrix, and the surface of the fibers wrinkles into rough one with some Si NPs clearly observable as highlighted in those dash circles (Figure 2b). The SEM cross sectional view, as shown in Figure 2c, verifies that it is constructed by highly porous thin C-PDA network inside the fibers. The Si NPs are uniformly and fully trapped in the network, as confirmed by the TEM image (Figure 2d) and the corresponding EDX-STEM elemental mapping (Figures 2g∼2i), and the individual Si nanoparticles are covered by C-PDA thin layer with some voids created in-between (Figure 2e). The coverage ensures efficient contact between Si and C-PDA for smooth electron conduction due to the high electrical conductivity of C-PDA with multilayered graphene structure,[45] while the voids allows electrolyte diffusion for ion transportation. The high-resolution TEM image, as shown in Figure 2f, further confirms the C-PDA coverage and the voids. In addition to the C-PDA thin layer, an extra layer with thickness of several nanometers is attached tightly onto the surface of Si NPs (Figure 3a). The XPS Si scanning of the sample, as shown in Figure 3b, verifies that this extra layer is silicon oxide (SiO_x), which is the native oxidized layer on the commercial Si NPs (Figure S1). The native SiO_x thin layer is beneficial for suppressing the volume expansion of the Si NPs during discharge/charge process.[46,47] Despite the formation of the SiO_x layer and that elemental Si is not detected in XPS pattern, which is probably due to the detection depth of XPS technique (< 10 nm) as well as the fact that the Si NPs are trapped within C-PDA network and covered by SiO_x layer, the majority is still elemental Si as confirmed by the XRD result (Figure 3c) which verifies the only face-centered cubic crystalline phase of Si.[48] The crystalline lattice of [111] with inter-spacing of about 0.31 nm is directly observed in Figure 3a. As mentioned above, the C-PDA/Si hybrids with different C-PDA thickness were prepared via varying the coating times, 2, 4 and 6. For the other two samples, C-PDA/Si-2t and C-PDA/Si-6t, similar morphologies and structures were observed (Figure S2 ∼ S4), while the larger C-PDA thin layer thickness gives rise to smoother surface of the fibers as well as lower Si content. As indicated in Figure 3d, the

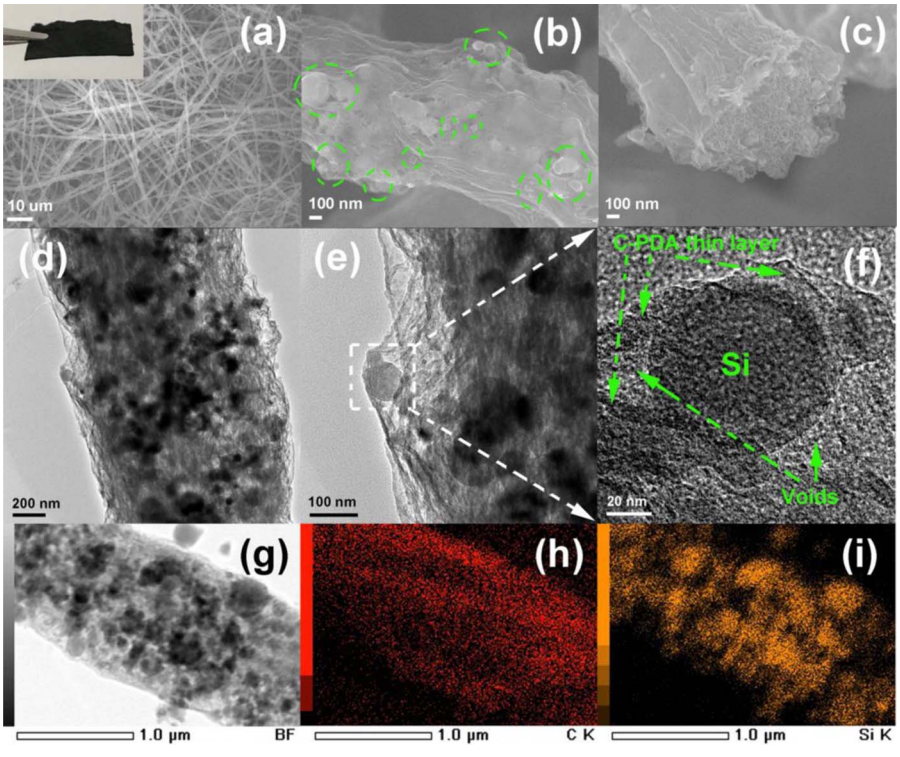

Figure 2. (a ∼ c) SEM and (d ∼ f) TEM images of Si NPs encapsulated in thin C-PDA network, taking C-PDA/Si-4t as a typical example. (g ∼ i) EDX-STEM elemental mapping of C and Si on a single C-PDA/Si fiber, showing the distribution.

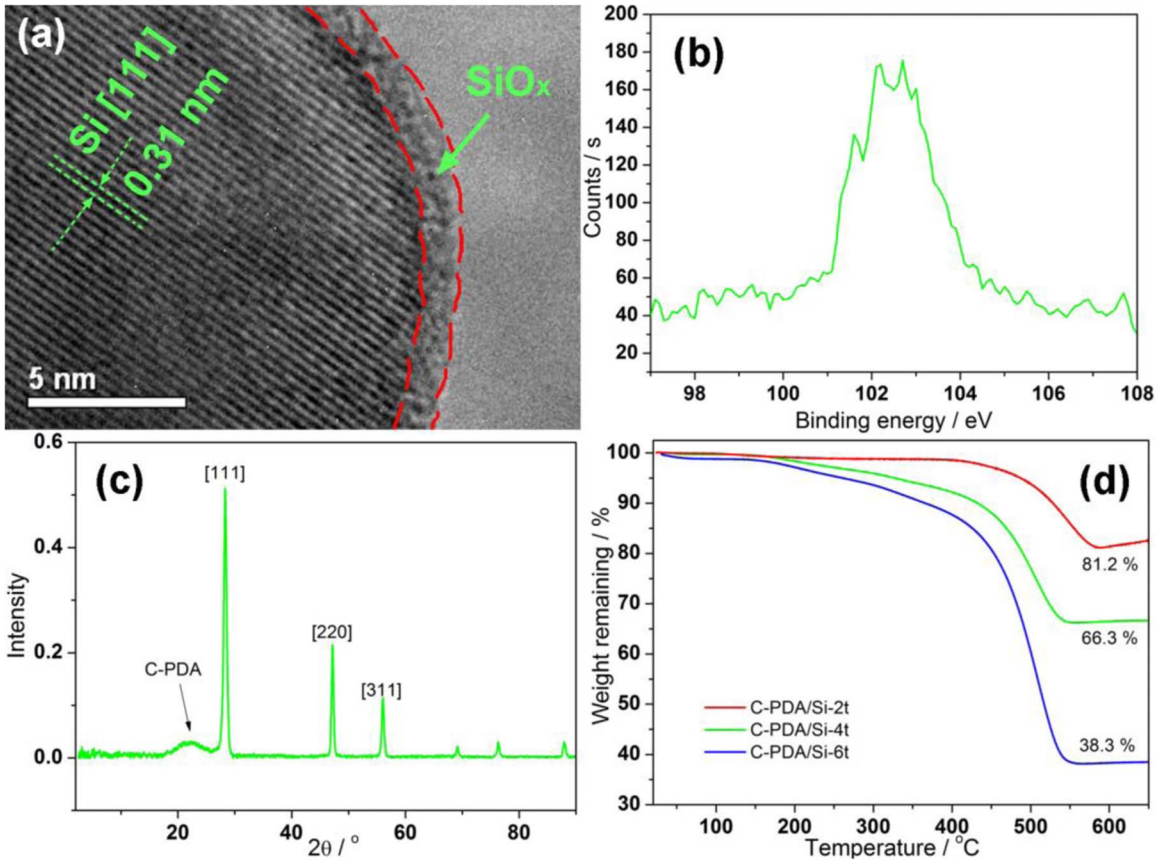

Figure 3. (a) TEM image of a single trapped Si nanoparticle, showing the crystalline structure as well as the formed SiO_x layer, (b) XPS pattern and (c) XRD result of C-PDA/Si-4t, and (d) TGA curves of the samples with different C-PDA thin layer thickness.

Si content in C-PDA/Si-2t, C-PDA/Si-4t and C-PDA/Si-6t is around 81.2, 66.3 and 38.3 wt%, respectively.

Electrochemical properties evaluation.—Herein, the strategy of confining Si NPs within a porous C-PDA thin layer network has been successfully verified as discussed above. The C-PDA/Si network is in freestanding form with high flexibility and good mechanical strength to sustain the cutting and battery assembling without using any binder and conductive agent. As anode of LIBs, the C-PDA/Si networks with different C-PDA thin layer thicknesses, i.e., varied Si contents, exhibit typical Si lithium/de-lithium behavior as confirmed by the CV results of C-PDA/Si-4t (Figure 4) within the voltage window of 1.5 ~ 0 V and scanning rate of 0.5 mV/S. The broad peak at around 0.5 V at the 1st lithiation curve, which disappears in the following lithiation curves, indicates the irreversible formation of solid electrolyte interphase (SEI) layer on the surface of anode. The shoulder at the lower voltage range of 1st lithiation curve, is attributed to the reversible alloying of lithium ions with Si. Two peaks located at about 0.37 and 0.58 V of the de-lithiation curves confirm the decomposition of the Li-Si alloy.[49,50] It is worth noting that the intensity of the reversible peaks on both cathodic and anodic curves increases along with the cycles, indicating that the lithium ions insertion into the anode may be a gradual process, and the activation of the Si takes place at the initial cycles. The charge/discharge capacity of the samples under the current density of 100 mA g^{-1} and voltage window of 1.5 ~ 0.005 V further verifies this. The charge-discharge curves for the 1st ~ 10th cycle, taking C-PDA/Si-4t as a typical example, as well as the cycled capacity of the samples are shown in Figures 5a and 5b. The charge-discharge behavior of the C-PDA/Si network is consistent with the CV results as analyzed above. It is clear that for all the three samples, the charge/discharge capacities keep increasing at the first 15 cycles, indicating that the Si is gradually activated during these cycles. Comparing the three, the one from 4 times PDA coating (C-PDA/Si-4t), i.e. with Si content of about 66.3 wt%, exhibits the best cycled capacity. The capacity remains at about 1750 mAh g^{-1} after 100 cycles under the testing condition. At higher current density of 200, 500, 1000 and 2000 mA g^{-1}, the C-PDA/Si-4t possesses capacity of around 1600 ~ 1700, 1200 ~ 1300, 800 ~ 900 and 600 ~ 700 mAh g^{-1}, respectively, and its capacity rebounds back to 1300 ~ 1500 mAh g^{-1} when the current density of 200 mA g^{-1} is applied again (Figure 5c). This indicates the good electrochemical performance, including stable cycled capacity and high rate capacity, of C-PDA/Si-4t. The much better

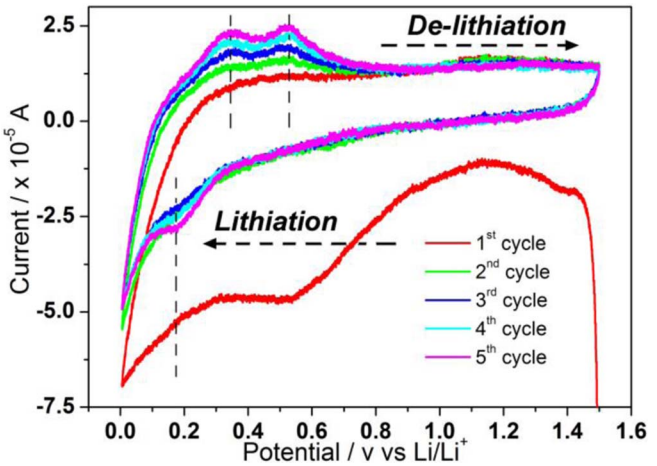

Figure 4. Cyclic voltammetric (CV) curves of C-PDA/Si-4t at the first 5 cycles.

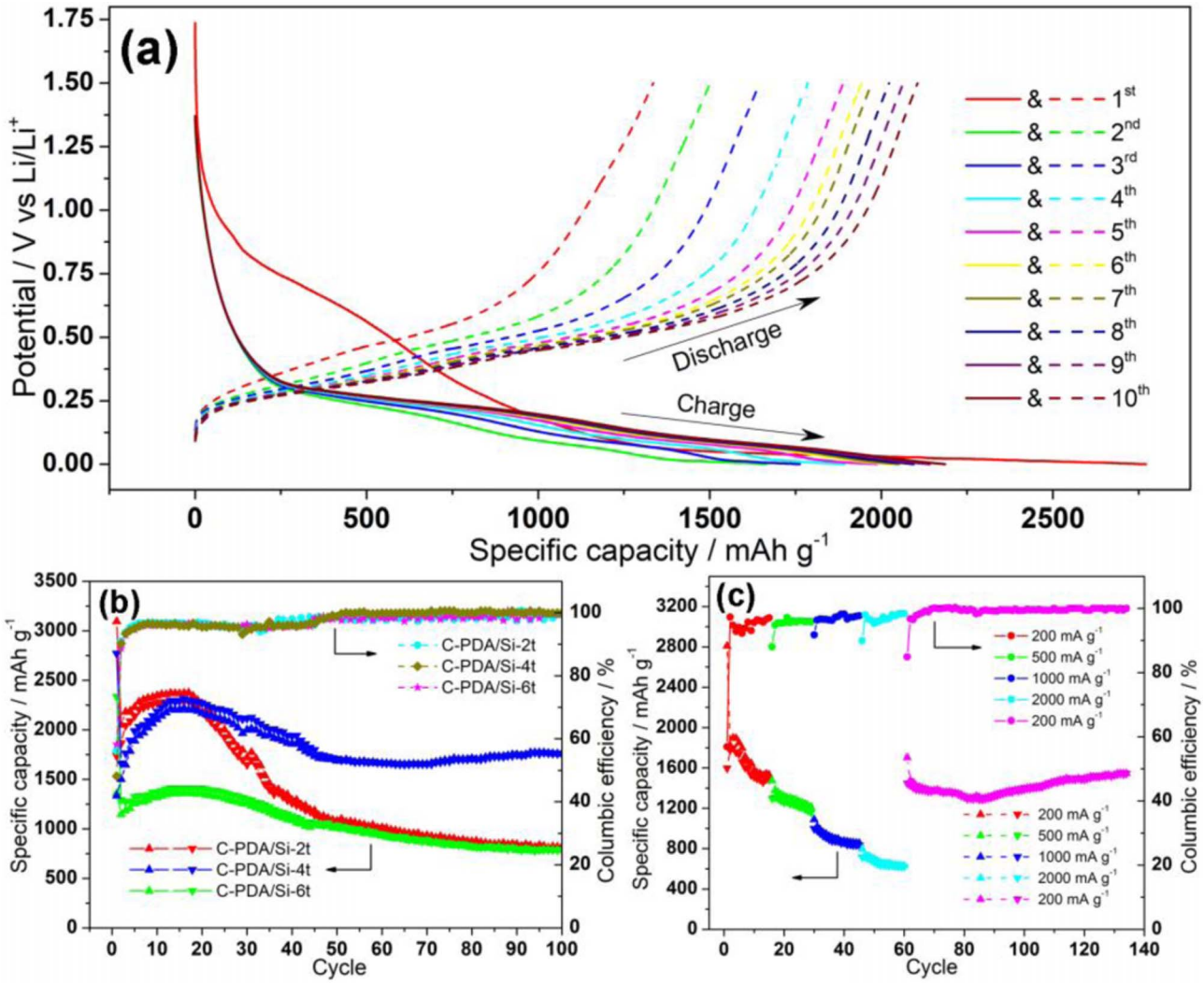

Figure 5. (a) Charge-discharge profiles of the samples under current density of 100 mA g^{-1}, taking the one with 4 times PDA coating as an example (C-PDA/Si-4t), and (b) cycled capacity of the samples under current density of 100 mA g^{-1}, and (c) rate capacity of the sample with 4 times PDA coating (C-PDA/Si-4t) under varied current density.

electrochemical property of C-PDA/Si-4t than that of the other two, C-PDA/Si-2t and C-PDA/Si-6t, is mainly ascribed to that the C-PDA network in C-PDA/Si-2t is too thin and brittle to accommodate the volume expansion of Si during lithiation/de-lithiation, resulting in carbon network cracking after cycling as confirmed in Figures 6a_1 and 6a_2, while the Si content in C-PDA/Si-6t is too low (38.3 wt%) to favor high electrochemical activity for Li ion alloying/de-alloying, despite that the structural integrity remains after cycling for both C-PDA/Si-4t and C-PDA/Si-6t (Figures 6b_1, 6b_2, 6c_1 and 6c_2). Furthermore, the thickness of the electrically conductive C-PDA thin layer may affect the ions insertion and transportation on the electrolyte solution-anode interface and within the anode, for which the thin layer with too small thickness conducts ions in a discontinuous manner during discharge/charge cycles, while that with too large thickness (normally $>$ 15 nm) hinders the transportation of ions. Therefore an appropriate thickness is required to conduct ions at low resistance. As clearly confirmed by the EIS results of the three anodes (Figure 7), the one from C-PDA/Si-4t possesses the lowest interfacial and ion diffusion resistance, leading to best electrochemical performance among all as presented above.

Morphological evolution upon lithiation and recyclability investigation.—Despite that the C-PDA is also electrochemically active and may alloy/de-alloy with Li ions during charging/discharging process,[43] the porous network contributes in a limited extent to the overall capacity due to the relatively low capacity as well as the low content. Nevertheless, the excellent electrical conductivity of C-PDA, which is intrinsically nitrogen-doped multilayered graphene,[45] creates continuous pathway for electron conduction. And the interconnected nanochannels within the C-PDA network allows free diffusion of electrolyte therefore the smooth transportation of Li ions into/from anode. This is schematically demonstrated in Scheme 2. Regarding the Li insertion/extraction of Si, it has been well known that a volume expansion of 300 $\sim$ 400% occurs upon Li-Si alloying, and the proper introduction of "breathable" carbon is to accommodate/buffer such volume change of Si for stable reversible cycling. Interestingly in this design, the expanded volume of Li-Si alloy is not simply buffered by the C-PDA thin layer. Instead, as can be seen from the TEM images (a_1, a_2, b_1 and b_2) after 1st charging in Scheme 2, the Si NPs collapsed into much smaller ones after lithiation. This is probably due to that the C-PDA thin layer constrains the volume expansion of the Si NPs in their respective frames during alloying with Li ions, and the stable C-PDA network acts as interlock to prevent the Li-Si alloy from further "growing" once the limited interspace of the C-PDA frame is fully filled, leading to the collapse of the Si due to the induced "expansion force" by the C-PDA network, as shown schematically in Scheme 2. The maintaining of the interspace size after 1st charging as in the TEM images (a_1 and b_1) further confirms that there is no volume change for

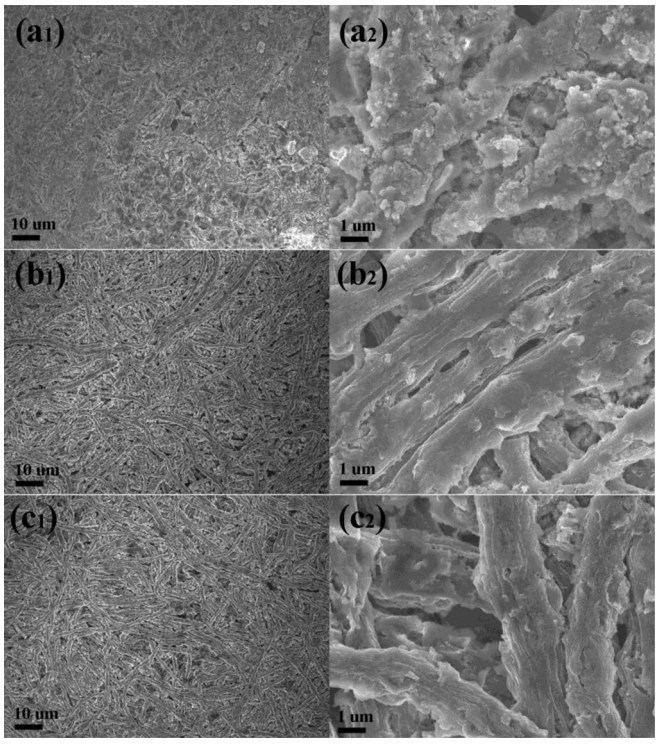

Figure 6. Morphology of the sample of (a_1 and a_2) C-PDA/Si-2t, (b_1 and b_2) C-PDA/Si-4t and (c_1 and c_2) C-PDA/Si-6t after cycling, showing the structure collapse in C-PDA/Si-2t and the structure integrity of the other two.

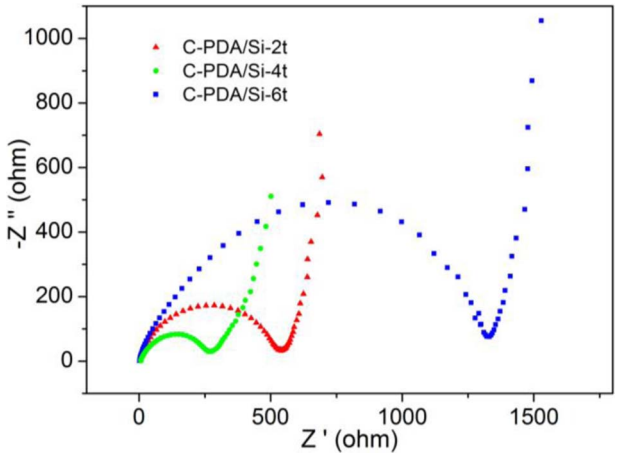

Figure 7. The electrochemical impedance spectroscopy (EIS) results of the batteries using C-PDA/Si-2t, C-PDA/Si-4t and C-PDA/Si-6t as anode.

the C-PDA frames, and the STEM-EDX elemental mapping results (Figures $8a_1 \sim 8a_3$) indicate the uniform distribution of Si within the network. Despite the collapse, the collapsed smaller Si is still completely trapped within the C-PDA frames since the outer surface of the C-PDA fibers is mostly enclosed without open pores (Figure 2b), and therefore stabilized by the C-PDA network, leading to good electrochemical performance in the following charging/discharging cycles. It is worth noting that the collapse of the Si NPs may not be finished within the 1st cycle but the initial few cycles. This explains why the capacity at the initial stage of until about 15th cycle keeps increasing along the cycles.

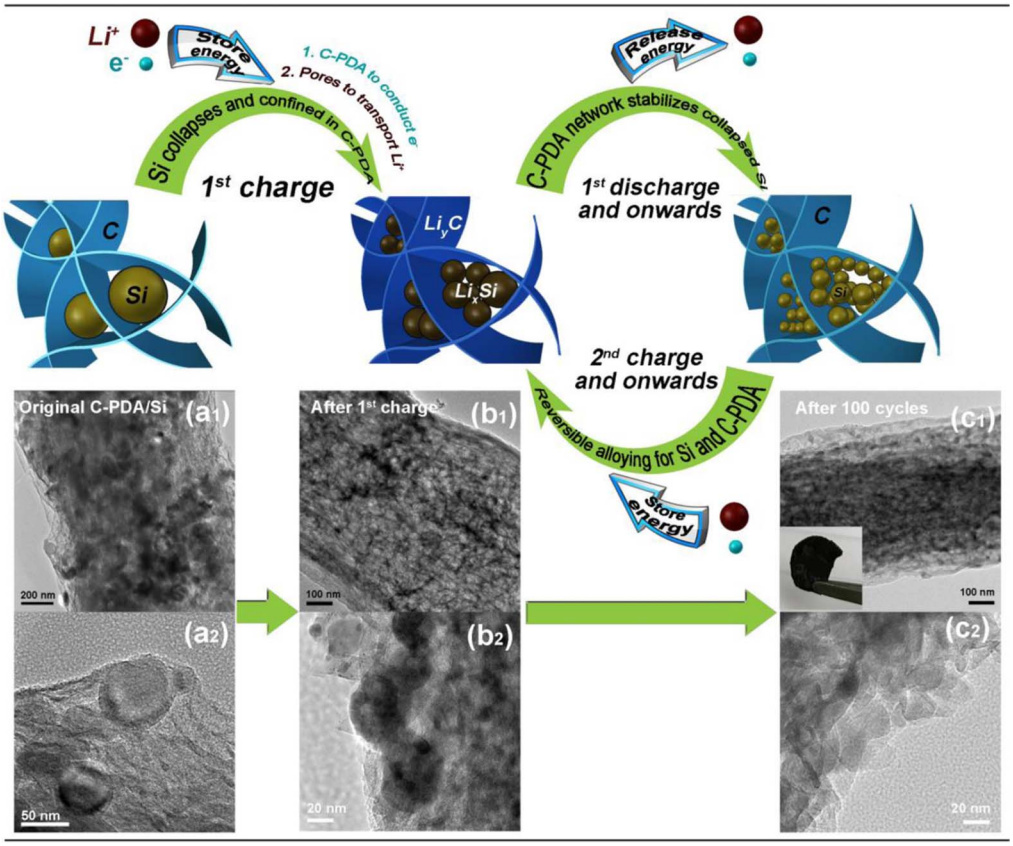

Scheme 2. Schematic demonstration of the lithiation/de-lithiation process of the C-PDA/Si network as well as the functionality of each component, and the corresponding TEM images of the C-PDA/Si network (C-PDA/Si-4t) after charging/discharging.

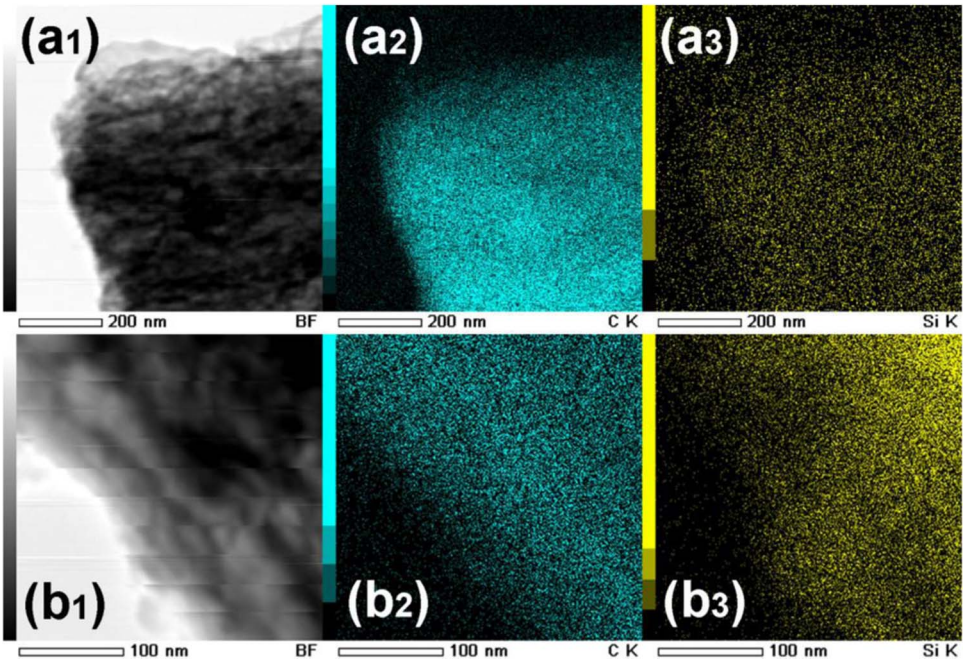

Figure 8. STEM-EDX elemental mapping (C, Si) of the C-PDA/Si-4t after ($a_1 \sim a_3$) 1st charging and ($b_1 \sim b_3$) 100 cycles.

The recyclability of the used anode was further investigated after 100 cycles. After cycling, the freestanding anode mat remains and can be easily peeled off from the current collector after disassembling the battery cell. The mat is mechanically strong enough to go with solvent washing and soaking process in order to remove the electrolyte, lithium compounds and other possible impurities, as shown in the inset of TEM image c_1 in Scheme 2. After purification through simple ethanol soaking for several times, the C-PDA network still maintains its fibrous integrity, and the Si NPs with much smaller size remain within the network (TEM image c_1 and c_2, Scheme 2), which is confirmed by the STEM-EDX elemental mapping results (Figures $8b_1 \sim 8b_3$). The TGA curve and XRD pattern of the sample (Figures 9a and 9b), C-PDA/Si-4t, after 100 cycle test and purification verifies the remained crystalline Si phase with high content of 59.5 wt%, close to the one before cycling (66.3 wt%). Comparing with the conventional paste-based anode made from powder, from which it is difficult and very troublesome to separate the active material from the binder, conductive agent and lithium compounds while maintaining the structural/morphological integrity of the material, the designed hybrid in this work can easily "recover" to almost original status through simple soaking and washing process. The recycled Si/C-PDA hybrid can be further used in other proper applications, or to retrieve Si compound upon burning C-PDA out.

Conclusions

A straightforward strategy has been designed in this work to utilize commercially available Si NPs as anode of LIBs directly by forming freestanding flexible and robust mat. The Si NPs were confined within the network of thin graphitized carbon (C-PDA) layer with significant interconnected nanochannels. The morphologies and structures of the C-PDA/Si network have been well studied, and the composition has been optimized based on electrochemical properties. Excellent electrochemical performance, including high cycled capacity and high rate capacity, has been achieved. This is due to the formation of highly electrically conductive C-PDA pathway for electron conduction and the interconnected nanochannels for Li ions transportation. A different phenomenon for the lithiation/de-lithiation of the Si compound was observed. Upon repeated lithiation/de-lithiation, the Si NPs collapse into smaller ones and are still trapped within the C-PDA frames. The smaller Si is further stabilized by the C-PDA network which acts as

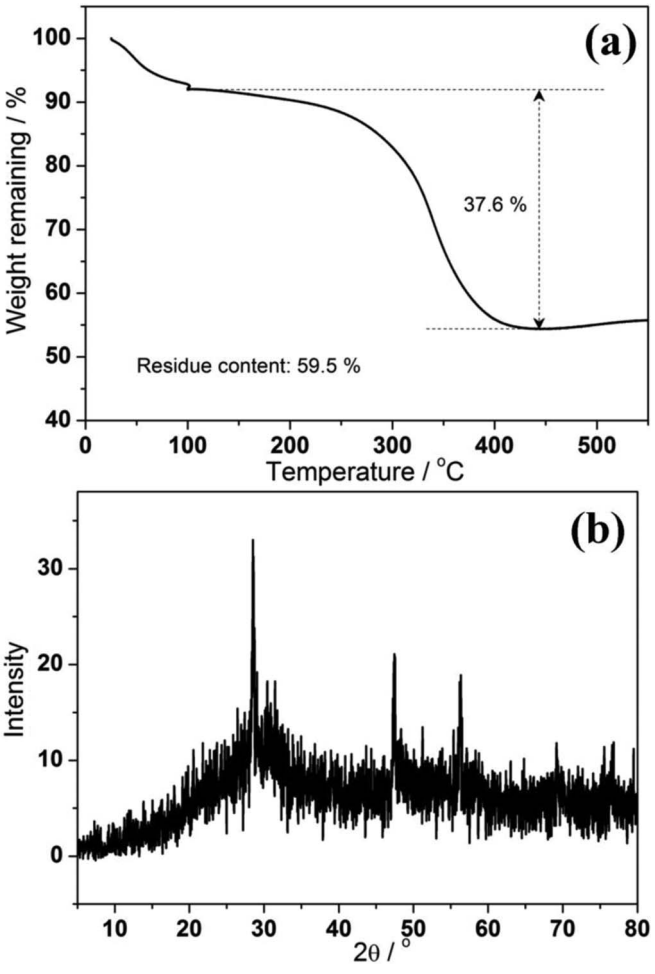

Figure 9. The (a) TGA curve and (b) XRD pattern of the C-PDA/Si-4t after 100 cycles test and purification, confirming the remained crystalline Si phase with relatively high content after cycling.

interlock, leading to good electrochemical performance. The recyclability of the obtained Si/C-PDA hybrid was further investigated after cycling test, suggesting that the designed hybrid can be easily recycled and reused due to its robust freestanding nature which requires no binder and conductive agent.

ORCID

Junhua Kong https://orcid.org/0000-0002-5296-6603
Yuefan Wei https://orcid.org/0000-0003-3050-1589

References

1. K. Feng, M. Li, W. W. Liu, A. G. Kashkooli, X. C. Xiao, M. Cai, and Z. W. Chen, Silicon-Based Anodes for Lithium-Ion Batteries: From Fundamentals to Practical Applications, *Small*, **14**, 33 (2018).
2. A. Casimir, H. G. Zhang, O. Ogoke, J. C. Amine, J. Lu, and G. Wu, Silicon-based anodes for lithium-ion batteries: Effectiveness of materials synthesis and electrode preparation, *Nano Energy*, **27**, 359 (2016).
3. M. Ashuri, Q. R. He, and L. L. Shaw, Silicon as a potential anode material for Li-ion batteries: where size, geometry and structure matter, *Nanoscale*, **8**, 74 (2016).
4. M. Gu, Y. He, J. M. Zheng, and C. M. Wang, Nanoscale silicon as anode for Li-ion batteries: The fundamentals, promises, and challenges, *Nano Energy*, **17**, 366 (2015).
5. X. Su, Q. L. Wu, J. C. Li, X. C. Xiao, A. Lott, W. Q. Lu, B. W. Sheldon, and J. Wu, Silicon-Based Nanomaterials for Lithium-Ion Batteries: A Review, *Adv. Energy Mater.*, **4**, 1300882 (2014).
6. M. T. McDowell, S. W. Lee, W. D. Nix, and Y. Cui, 25th Anniversary Article, Understanding the Lithiation of Silicon and Other Alloying Anodes for Lithium-Ion Batteries, *Adv. Mater.*, **25**, 4966 (2013).
7. F. Luo, B. Liu, J. Zheng, G. Chu, K. Zhong, H. Li, X. Huang, and L. Chen, Review—Nano-Silicon/Carbon Composite Anode Materials Towards Practical Application for Next Generation Li-Ion Batteries, *J. Electrochem. Soc.*, **162**, A2509 (2015).
8. C. Liu, Y. Zhao, R. Yi, Y. Sun, Y. Li, L. Yang, I. Mitrovic, S. Taylor, P. Chalker, and C. Zhao, Alloyed Cu/Si core-shell nanoflowers on the three-dimensional graphene foam as an anode for lithium-ion batteries, *Electrochim. Acta*, **306**, 45 (2019).
9. H. Gao, L. S. Xiao, I. Plume, G. L. Xu, Y. Ren, X. B. Zuo, Y. Z. Liu, C. Schulz, H. Wiggers, K. Amine, and Z. H. Chen, Parasitic Reactions in Nanosized Silicon Anodes for Lithium-Ion Batteries, *Nano Letters*, **17**, 1512 (2017).
10. X. H. Zhang, X. Y. Qiu, D. B. Kong, L. Zhou, Z. H. Li, X. L. Li, and L. J. Zhi, Silicene Flowers: A Dual Stabilized Silicon Building Block for High-Performance Lithium Battery Anodes, *ACS Nano*, **11**, 7476 (2017).
11. T. Yoon, T. Bok, C. Kim, Y. Na, S. Park, and K. S. Kim, Mesoporous Silicon Hollow Nanocubes Derived from Metal-Organic Framework Template for Advanced Lithium-Ion Battery Anode, *ACS Nano*, **11**, 4808 (2017).
12. P. Gao, H. Tang, A. Xing, and Z. Bao, Porous silicon from the magnesiothermic reaction as a high-performance anode material for lithium ion battery applications, *Electrochim. Acta*, **228**, 545 (2017).
13. G. C. Shivaraju, C. Sudakar, and A. S. Prakash, High-rate and long-cycle life performance of nano-porous nano-silicon derived from mesoporous MCM-41 as an anode for lithium-ion battery, *Electrochim. Acta*, **294**, 357 (2019).
14. J. B. Cook, H. S. Kim, T. C. Lin, S. Robbennolt, E. Detsi, B. S. Dunn, and S. H. Tolbert, Tuning Porosity and Surface Area in Mesoporous Silicon for Application in Li-Ion Battery Electrodes, *ACS Appl. Mater. Interfaces*, **9**, 19063 (2017).
15. R. V. Salvatierra, A. R. O. Raji, S. K. Lee, Y. S. Ji, L. Li, and J. M. Tour, Silicon Nanowires and Lithium Cobalt Oxide Nanowires in Graphene Nanoribbon Papers for Full Lithium Ion Battery, *Adv. Energy Mater.*, **6**, 1600918 (2016).
16. M. R. Zamfir, H. T. Nguyen, E. Moyen, Y. H. Lee, and D. Pribat, Silicon nanowires for Li-based battery anodes: a review, *J. Mater. Chem. A*, **1** 9566 (2013).
17. W. Weng and W. Xiao, Electrodeposited Silicon Nanowires from Silica Dissolved in Molten Salts as a Binder-Free Anode for Lithium-Ion Batteries, ACS Appl. *Energy Mater.*, **2**, 804 (2019).
18. A. Krause, O. Tkacheva, A. Omar, U. Langklotz, L. Giebeler, S. Dörfler, F. Fauth, T. Mikolajick, and W. M. Weber, In Situ Raman Spectroscopy on Silicon Nanowire Anodes Integrated in Lithium Ion Batteries, *J. Electrochem. Soc.*, **166**, A5378 (2019).
19. Q. Hao, J. Hou, J. Ye, H. Yang, J. Du, and C. Xu, Hierarchical macroporous Si/Sn composite: Easy preparation and optimized performances toward lithium storage, *Electrochim. Acta*, **306**, 427 (2019).
20. R. Fu, P. Nie, M. Shi, J. Wang, J. Jiang, Y. Zhang, Y. Wu, S. Fang, H. Dou, and X. Zhang, Rigid Polyimide Buffering Layer Enabling Silicon Nanoparticles Prolonged Cycling Life for Lithium Storage, *ACS Appl. Energy Mater.*, **1**, 948 (2018).
21. J. M. Whiteley, J. W. Kim, D. M. Piper, and S.-H. Lee, High-Capacity and Highly Reversible Silicon-Tin Hybrid Anode for Solid-State Lithium-Ion Batteries, *J. Electrochem. Soc.*, **163**, A251 (2016).
22. M. Kummer, J. P. Badillo, A. Schmitz, H.-G. Bremes, M. Winter, C. Schulz, and H. Wiggers, Silicon/Polyaniline Nanocomposites as Anode Material for Lithium Ion Batteries, *J. Electrochem. Soc.*, **161**, A40 (2014).
23. X. X. Ma, G. M. Hou, Q. Ai, L. Zhang, P. C. Si, J. K. Feng, and L. J. Ci, A heart-coronary arteries structure of carbon nanofibers/graphene/silicon composite anode for high performance lithium ion batteries, *Sci. Rep.*, **7**, 9642 (2017).
24. X. S. Zhou, L. J. Wan, and Y. G. Guo, Electrospun Silicon Nanoparticle/Porous Carbon Hybrid Nanofibers for Lithium-Ion Batteries, *Small*, **9**, 2684 (2013).
25. J. Kong, W. A. Yee, Y. Wei, L. Yang, J. M. Ang, S. L. Phua, S. Y. Wong, R. Zhou, Y. Dong, X. Li, and X. Lu, Silicon nanoparticles encapsulated in hollow graphitized carbon nanofibers for lithium ion battery anodes, *Nanoscale*, **5**, 2967 (2013).
26. S. Palumbo, L. Silvestri, A. Ansaldo, R. Brescia, F. Bonaccorso, and V. Pellegrini, Silicon-Few Layer Graphene Nanocomposite as High-Capacity and High-Rate Anode in Lithium-Ion Batteries, *ACS Appl. Energy Mater.*, (2019).
27. S. Suresh, Z. P. Wu, S. F. Bartolucci, S. Basu, R. Mukherjee, T. Gupta, P. Hundekar, Y. F. Shi, T. M. Lu, and N. Koratkar, Protecting Silicon Film Anodes in Lithium-Ion Batteries Using an Atomically Thin Graphene Drape, *ACS Nano*, **11**, 5051 (2017).
28. N. Kim, S. Chae, J. Ma, M. Ko, and J. Cho, Fast-charging high-energy lithium-ion batteries via implantation of amorphous silicon nanolayer in edge-plane activated graphite anodes, *Nat. Commun.*, **8**, 10 (2017).
29. S. Q. Huang, L. Z. Cheong, D. Y. Wang, and C. Shen, Nanostructured Phosphorus Doped Silicon/Graphite Composite as Anode for High-Performance Lithium-Ion Batteries, *ACS Appl. Mater. Interfaces*, **9**, 23672 (2017).
30. E. Greco, G. Nava, R. Fathi, F. Fumagalli, A. E. Del Rio-Castillo, A. Ansaldo, S. Monaco, F. Bonaccorso, V. Pellegrini, and F. Di Fonzo, Few-layer graphene improves silicon performance in Li-ion battery anodes, *J. Mater. Chem. A*, **5**, 19306 (2017).
31. X. Zhao, C.-H. Yim, N. Du, and Y. Abu-Lebdeh, Crosslinked Chitosan Networks as Binders for Silicon/Graphite Composite Electrodes in Li-Ion Batteries, *J. Electrochem. Soc.*, **165**, A1110 (2018).
32. P. Fan, T. Mu, S. Lou, X. Cheng, Y. Gao, C. Du, P. Zuo, Y. Ma, and G. Yin, Amorphous carbon-encapsulated Si nanoparticles loading on MCMB with sandwich structure for lithium ion batteries, *Electrochim. Acta*, **306**, 590 (2019).
33. H. P. Su, A. A. Barragan, L. X. Geng, D. H. Long, L. C. Ling, K. N. Bozhilov, L. Mangolini, and J. C. Guo, Colloidal Synthesis of Silicon-Carbon Composite Material for Lithium-Ion Batteries, *Angew. Chem.-Int. Edit.*, **56**, 10780 (2017).
34. M. G. Jeong, H. L. Du, M. Islam, J. K. Lee, Y. K. Sun, and H. G. Jung, Self-Rearrangement of Silicon Nanoparticles Embedded in Micro Carbon Sphere Framework for High-Energy and Long-Life Lithium Ion Batteries, *Nano Letters*, **17**, 5600 (2017).
35. S. Q. Chen, L. F. Shen, P. A. van Aken, J. Maier, and Y. Yu, Dual-Functionalized Double Carbon Shells Coated Silicon Nanoparticles for High Performance Lithium-Ion Batteries, *Adv. Mater.*, **29**, 1605650 (2017).
36. C. Gao, H. Zhao, J. Wang, J. Wang, C. Yan, and H. Yin, Self-Assembly of Hierarchical Silicon Suboxide Nanoparticles Encapsulated in Nitrogen-Doped Carbon as High Performance Anode Material for Lithium-Ion Batteries, *J. Electrochem. Soc.*, **166**, A574 (2019).
37. D. Mazouzi, R. Grissa, M. Paris, Z. Karkar, L. Huet, D. Guyomard, L. Roué, T. Devic, and B. Lestriez, CMC-citric acid Cu(II) cross-linked binder approach to improve the electrochemical performance of Si-based electrodes, *Electrochim. Acta*, **304**, 495 (2019).
38. S. Choi, T. W. Kwon, A. Coskun, and J. W. Choi, Highly elastic binders integrating polyrotaxanes for silicon microparticle anodes in lithium ion batteries, *Science*, **357**, 4 (2017).
39. A. Urbanski, A. Omar, J. Guo, A. Janke, U. Reuter, M. Malanin, F. Schmidt, D. Jehnichen, M. Holzschuh, F. Simon, K.-J. Eichhorn, L. Giebeler, and P. Uhlmann, An Efficient Two-Polymer Binder for High-Performance Silicon Nanoparticle-Based Lithium-Ion Batteries: A Systematic Case Study with Commercial Polyacrylic Acid and Polyvinyl Butyral Polymers, *J. Electrochem. Soc.*, **166**, A5275 (2019).
40. S. Lawes, Q. Sun, A. Lushington, B. W. Xiao, Y. L. Liu, and X. L. Sun, Inkjet-printed silicon as high performance anodes for Li-ion batteries, *Nano Energy*, **36**, 313 (2017).
41. J. H. Kong, C. Y. Zhao, Y. F. Wei, S. L. Phua, Y. L. Dong, and X. H. Lu, Nanocups-on-microtubes: a unique host toward high-performance lithium ion batteries, *J. Mater. Chem. A*, **2**, 15191 (2014).
42. C. L. Pai, M. C. Boyce, and G. C. Rutledge, Morphology of Porous and Wrinkled Fibers of Polystyrene Electrospun from Dimethylformamide, *Macromolecules*, **42**, 2102 (2009).
43. J. Kong, C. Zhao, Y. Wei, and X. Lu, MoS2 Nanosheets Hosted in Polydopamine-Derived Mesoporous Carbon Nanofibers as Lithium-Ion Battery Anodes: Enhanced MoS2 Capacity Utilization and Underlying Mechanism, *ACS Appl. Mater. Interfaces*, **7**, 24279 (2015).
44. J. Kong, X. Yao, Y. Wei, C. Zhao, J. M. Ang, and X. Lu, Polydopamine-derived porous nanofibers as host of $ZnFe_2O_4$ nanoneedles: toward high-performance anodes for lithium-ion batteries, *RSC Adv.*, **5**, 13315 (2015).
45. J. Kong, W. A. Yee, L. Yang, Y. Wei, S. L. Phua, H. G. Ong, J. M. Ang, X. Li, and X. Lu, Highly electrically conductive layered carbon derived from polydopamine and its functions in SnO_2-based lithium ion battery anodes, *Chem. Commun.*, **48**, 10316 (2012).
46. M. T. McDowell, S. W. Lee, I. Ryu, H. Wu, W. D. Nix, J. W. Choi, and Y. Cui, Novel Size and Surface Oxide Effects in Silicon Nanowires as Lithium Battery Anodes, *Nano Lett.*, **11**, 4018 (2011).
47. S. Sim, P. Oh, S. Park, and J. Cho, Critical Thickness of SiO2 Coating Layer on Core@Shell Bulk@Nanowire Si Anode Materials for Li-Ion Batteries, *Adv. Mater.*, **25**, 4498 (2013).
48. H. Ma, F. Cheng, J. Y. Chen, J. Z. Zhao, C. S. Li, Z. L. Tao, and J. Liang, Nest-like Silicon Nanospheres for High-Capacity Lithium Storage, *Adv. Mater.*, **19**, 4067 (2007).
49. R. Huang, X. Fan, W. Shen, and J. Zhu, Carbon-coated silicon nanowire array films for high-performance lithium-ion battery anodes, *Appl. Phys. Lett.*, **95**, 133119 (2009).
50. Y. Yao, M. T. McDowell, I. Ryu, H. Wu, N. Liu, L. Hu, W. D. Nix, and Y. Cui, Interconnected Silicon Hollow Nanospheres for Lithium-Ion Battery Anodes with Long Cycle Life, *Nano Lett.*, **11**, 2949 (2011).